

Cite this: *Dalton Trans.*, 2021, **50**,
2585

Synthesis, crystal structures and magnetic properties of a P-stereogenic *ortho*-(4-amino-tempo)phosphinic amide radical and its Cu^{II} complex†

Yolanda Navarro,^a Guilherme P. Guedes,^b Miguel A. del Águila-Sánchez,^a
María José Iglesias,^a Francisco Lloret*^c and Fernando López-Ortiz *^a

The synthesis of phosphinic amides containing one 4-amino-TEMPO substituent at the *ortho* position has been achieved through copper(I) catalyzed cross-coupling reactions of *ortho*-iodophosphinic amides with 4-amino-TEMPO. The method has been extended to the preparation of the first example of a P-stereogenic *ortho*-(4-amino-tempo)phosphinic amide radical **10**. The reaction of **10** with Cu(hfac)₂ afforded the P-stereogenic Cu^{II} complex **19**. The crystal structure of both chiral compounds is reported. The molecular structure of **10** consists of a supramolecular zig-zag chain formed by intermolecular hydrogen bonds between the NH group of the phosphinic amide moiety and the nitroxide oxygen atom. In complex **19**, the ligand acts as a bridge between two Cu^{II} ions coordinated to the oxygen atoms of the P=O and N–O groups leading to the formation of a polymeric helicate chain in which the metal ions exist in a distorted octahedral geometry. The magnetic behavior of ligand **10** is characterized by very weak intermolecular anti-ferromagnetic interactions, whereas ferro- and anti-ferromagnetic interactions are present in complex **19**.

Received 18th December 2020,
Accepted 12th January 2021

DOI: 10.1039/d0dt04298f

rsc.li/dalton

Introduction

In recent decades, remarkable attention has been paid to molecular magnetism due to its applications in fields such as molecular spintronics, high-density data storage and quantum computing devices.¹ Thus, the design of molecular structures aimed at rational control of magnetic interactions between spin carriers has become a topic of great interest. Among them, chiral molecular magnets have been proven to be useful materials especially for the construction of advanced memory and logic devices due to their multiferroic, magnetization-induced second harmonic generation (MSHG) and magneto-chiral dichroism (MChD) effects² and are also interesting due to their potential applications in more diverse fields such as asymmetric catalysis, enantioselective separation and medicine.³ Persistent organic radicals play a key role as they are

paramagnetic stabilized compounds whose structure can be easily modified through organic synthesis methods, allowing the introduction of new properties and different coordination sites for the construction of complexes with a variety of topologies and functionalities. Nitronyl-nitroxides and nitroxides are two of the most used organic building blocks for this purpose, especially the TEMPO radical (2,2,6,6-tetramethylpiperidine-1-oxyl), from which a large number of derivatives have been synthesized with numerous interesting architectures and magnetic properties.⁴

The linkage between chirality and organic radical chemistry has found worthwhile applications in multiple fields such as enantioselective catalysis,⁵ molecular magnetism,⁶ liquid crystals⁷ and protective agents against oxidative stress.⁸ Chirality in organic radicals may be achieved by spontaneous resolution from achiral molecules that give rise to a chiral structure in the solid state,^{2b,9} or through the existence of atomic stereogenic centers, atropisomeric conformations, helical structures or a combination of elements of chirality.¹⁰ The usual approach for introducing chirality in molecular-based magnetic materials involves the use of enantiopure nitroxide and nitronyl nitroxide radicals containing C-stereogenic centers combined with coordination to paramagnetic metal ions.^{10,11} A wide variety of chiral nitronyl nitroxide-based radicals have been synthesized, from which some complexes have been reported (Fig. 1). Two isomers of a chiral nitronyl nitroxide

^aÁrea de Química Orgánica, Centro de Investigación CIAIMBITAL, Universidad de Almería, Carretera de Sacramento s/n, 04120 Almería, Spain. E-mail: flortiz@ual.es^bUniversidade Federal Fluminense, Instituto de Química, Departamento de Química Inorgânica, Niterói, Rio de Janeiro, Brazil^cInstitut de Ciència Molecular, Universitat de València, Catedràtic José Beltrán no.2, 46980 Paterna, Valencia, Spain† Electronic supplementary information (ESI) available: NMR spectra of the compounds synthesized and X-ray crystallographic data of **10** and **13**. CCDC 2011812 and 2011813. For ESI and crystallographic data in CIF or other electronic format see DOI: 10.1039/d0dt04298f

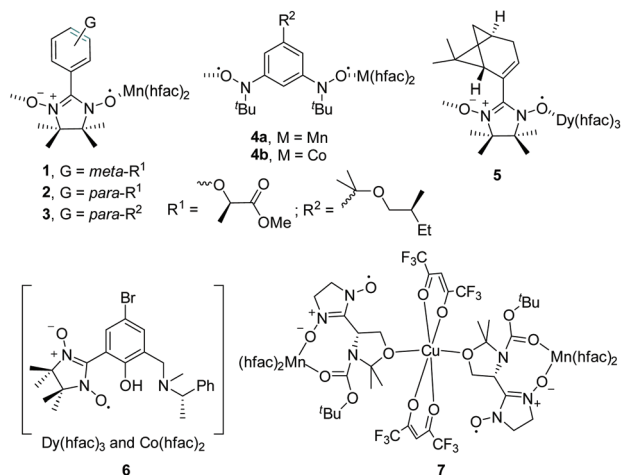


Fig. 1 Representative examples of chiral complexes based on the metal–radical approach.

radical have been used for the synthesis of manganese complexes **1** and **2**. Compound **1** is a polymeric 2₁ chain complex that acts as a ferrimagnet,¹² while compound **2** shows an helical-chain structure with a very low ratio between the intra-chain and interchain exchange parameters ($J'/J = 1.5 \times 10^{-5}$).¹³ Manganese complex **3** behaves as a ferrimagnet below $T_C = 5.0$ K, and complex **4a**,¹⁴ obtained from a chiral di-*tert*-butyl nitroxide radical, behaves as a metamagnet below $T_N = 5.4$ K. The same chiral radical was used for the synthesis of cobalt complex **4b**,¹⁵ from which a 1D helical-chain structure with antiferromagnetic interactions between paramagnetic sites was obtained. Complex **5** is the first example of a chiral lanthanide-radical compound combining optical chirality and magnetic anisotropy and shows SCM behaviour.¹⁶ Some heterometallic complexes have also been described. Compound **6** is a 2p–3d–4f complex showing SMM behaviour due to the Co^{II}–Rad exchange coupling interaction together with improved single ion magnetic properties of Co^{II} and Dy^{III} ions.¹⁷ For Mn–Cu–Rad complex **7**, a strong antiferromagnetic interaction between Mn and the organic radical was described, along with a much weaker antiferromagnetic interaction between the Mn(hfac)₂ unit and Cu(hfac)₂.¹⁸ A few examples of chiral verdazyl radicals have also been reported.¹⁹ However, to the best of our knowledge, there are no examples to date regarding the use of P-stereogenic compounds in molecular magnetism.²⁰

A number of P-containing TEMPO derivatives have been described to date, including phosphates, phosphoramidites, phosphazenes and phosphonates, among others.²¹ However, the use of these compounds in molecular magnetism has received little attention. Recently, our group has introduced a new phosphinic amide-TEMPO radical, 1-piperidinyloxy-4-[(diphenylphosphinyl)-amino]-2,2,6,6-tetramethyl radical (DPPNtempo), as a scaffold for the construction of achiral magnetic systems based on the coordination of the P=O/N–O[•] groups to the first row transition-metals²² such as Cu^{II}, Mn^{II} and Co^{II} and some lanthanides,²³ revealing the usefulness of

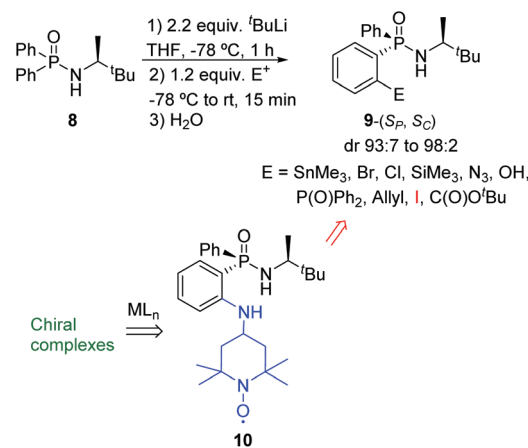
the functionalized radical to provide discrete or extended molecules with antiferromagnetic interactions between spin carriers. Interestingly, light emission properties were also observed for the terbium(III)-based complex, proving the potential of the compounds as multifunctional materials. Thus, we thought that the introduction of chirality through the phosphorus atom in these systems would provide chiral ligands that combined with paramagnetic metal ions would give rise to advanced multifunctional materials.

The synthesis of P-stereogenic compounds can be achieved in three different ways: nucleophilic or electrophilic attack on the phosphorus atom, or the desymmetrization of prochiral R₂P groups.²⁴ For the synthesis of P-stereogenic phosphinic amides, our group has developed very efficient methodologies based on the desymmetrization of prochiral Ph₂P groups of phosphinimidic amides²⁵ and phosphinic amides²⁶ through the highly diastereoselective *ortho* deprotonation of derivatives bearing C-chiral amino moieties and subsequent electrophilic trapping. The application of this procedure to phosphinic amide **8** provided access to a wide variety of P-stereogenic *ortho*-substituted compounds **9** in high yields and with excellent control (Scheme 1). We thought that this methodology could be extended to the synthesis of P-stereogenic nitroxide radicals by connecting a radical moiety at the *ortho* position of the chiral diphenylphosphinic amide framework taking advantage of the substituents introduced at the *ortho* position.

We describe herein the amination of *P*-(2-iodophenyl)-*P*-phenylphosphinic amides with 4-amino-TEMPO (ATEMPO) catalyzed by Cu^I salts to give *ortho*-alkylaminophosphinic amides and the application of the method to the synthesis of the first example of a P-stereogenic *ortho*-(4-amino-TEMPO) derivative **10** and its Cu^{II} complex.

Results and discussion

The strategies reported to introduce an ATEMPO radical to an aromatic ring include reductive amination using 4-oxo-TEMPO



Scheme 1 Synthesis of P-stereogenic phosphinic amides as the source of P-stereogenic TEMPO radicals and complexes.

as a carbonyl component²⁷ and S_NAr reactions in which ATEMPO acts as a nucleophile.²⁸ Reductive amination affords low yield and the reduction step may lead to the partial reduction of the radical. On the other hand, S_NAr reactions require the presence of strong electron-withdrawing substituents, such as nitro or imide, at the aromatic nucleus. For the synthesis of the radical compound **10**, a method based on the C–N cross-coupling reaction of the P-stereogenic *ortho* iodo derivative **9a** and the commercially available 4-amino-TEMPO **12** was developed.

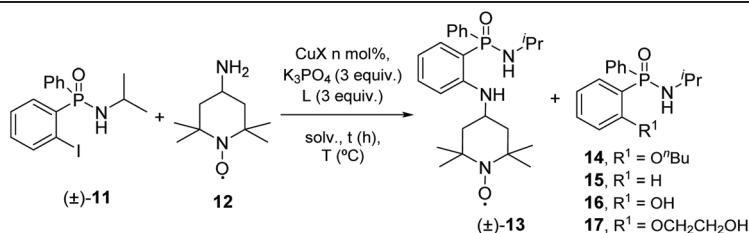
Firstly, the optimized reaction conditions for the amination of the racemic analogue (\pm)-**11** were investigated, due to the similarity of both the compounds and the greater simplicity of preparation. Palladium and copper are the most commonly used catalysts for C–N coupling reactions and some methodologies based on Ni(II) salts have also been described for similar systems.²⁹ For the reaction of *ortho*-iodophosphinic amide **11** with **12**, three different C–N coupling methodologies were tested using Ni(II),^{29a} Pd(II)³⁰ and Cu(I)³¹ salts as catalysts. Palladium and copper promoted the formation of the desired product, albeit in a very low yield. However, the palladium-catalyzed reaction afforded a larger number of by-products. For this reason, we focused on the method described by Buchwald *et al.*³¹ and made some modifications including the use of different salts, loading of catalysts, solvents, ligands, temperatures and reaction times in order to improve the results. The results are summarized in Table 1. The reaction of **11** with 1.2 equivalents of ATEMPO in the presence of 20% of CuI, three equiv. of ethylene glycol, and isopropanol as the solvent at 80 °C at a reaction time of 19 hours (entry 1)

afforded the desired product in a conversion of 22%, together with some by-products and 52% of the starting material. The formation of **13** was established based on the analysis of the NMR spectra of the crude mixture and was then corroborated by the isolation of the compound through flash column chromatography. The key aspect was the appearance of a highly shielded multiplet at δ_{H} 6.60 ppm in the ¹H NMR spectrum assigned to the *ortho* proton with respect to the amino group of the TEMPO moiety. This assignment was confirmed through the correlation observed in the ¹H,³¹P HMQC spectrum (optimized for the detection of connections *via* long-range coupling constants) between this proton and the ³¹P signal at δ_{P} = 29.6 ppm.

The increase of the reaction time to 48 h led to a decrease of the conversion to 13% (entry 2). Changing the solvent to ⁿBuOH allowed an increase in the temperature to 100 °C (entry 3). However, the use of less hindered alcohol favoured the formation of the C–O coupling compound **14** with the solvent as the major product (67%). The low melting point of the TEMPO radical (37–39 °C) is crucial in order to overcome this issue and to improve the efficiency of the process. Thus, in the absence of a solvent, the reaction of **11** with 10 equiv. of **12** for *ca.* 3 days afforded the desired product in a significantly higher conversion of 55% (entry 4).

Compounds **15**, **16** and **17** were also identified as by-products of the reaction in entry 4 (conversions of 17%, 8% and 20%, respectively). Product **15** arises from the reduction of the starting *ortho*-iodophosphinic amide in the reaction media, and the presence of phenol **16** can be explained by the cross-coupling of **11** with small amounts of water likely obtained

Table 1 Optimization of the coupling reaction of *ortho*-iodophosphinic amide **11** and ATEMPO



| | CuX | Mol% | Ligand (L) | Solvent | t (h) | T (°C) | Conversion ^a (%) |
|----------------|-------------------|------|---|-------------------|-------|--------|-----------------------------|
| 1 | CuI | 20 | (CH ₂) ₂ (OH) ₂ | <i>i</i> PrOH | 19 | 80 | 22 |
| 2 | CuI | 20 | (CH ₂) ₂ (OH) ₂ | <i>i</i> PrOH | 48 | 80 | 13 |
| 3 | CuI | 20 | (CH ₂) ₂ (OH) ₂ | ⁿ BuOH | 27 | 100 | 10 |
| 4 ^b | CuI | 20 | (CH ₂) ₂ (OH) ₂ | — | 69 | 100 | 55 |
| 5 | CuI | 50 | (CH ₂) ₂ (OH) ₂ | — | 69 | 100 | 13 |
| 6 | CuBr | 20 | (CH ₂) ₂ (OH) ₂ | — | 69 | 100 | 41 |
| 7 | CuCN | 20 | (CH ₂) ₂ (OH) ₂ | — | 69 | 100 | 50 |
| 8 | CuCN | 20 | <i>i</i> PrOH | — | 69 | 100 | 53 |
| 9 | CuCN | 10 | <i>i</i> PrOH | — | 69 | 90 | 63 |
| 10 | CuCN | 5 | <i>i</i> PrOH | — | 69 | 90 | 62 |
| 11 | CuCN | 5 | — | — | 69 | 90 | 50 |
| 12 | CuCN | 10 | <i>t</i> BuOH | — | 69 | 90 | 40 |
| 13 | Cu ₂ O | 10 | <i>i</i> PrOH | — | 69 | 90 | 64 |
| 14 | CuOAc | 10 | <i>i</i> PrOH | — | 69 | 90 | 72 |

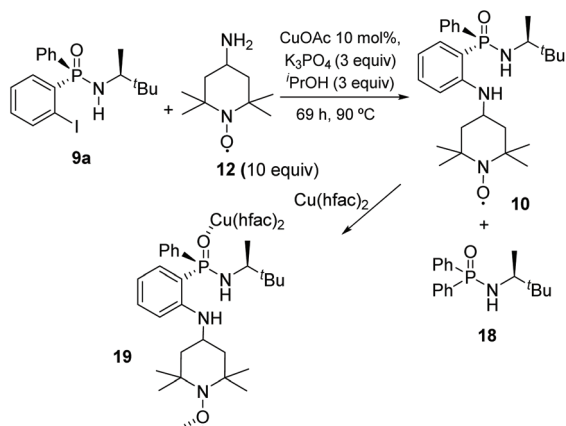
^a Determined by integration of the ³¹P NMR spectrum. ^b For solvent-less reactions (entries 4 to 14), 10 equivalents of **12** were used.

from slow diffusion during 3 days of the reaction. Analogously, compound **17** is generated from the C–O coupling of ethylene glycol which is used as the ligand with **11**, a behaviour similar to that observed in the reaction in the presence of *n*-butanol.

The increase of the loading of the catalyst to 50% was disadvantageous (entry 5). A cleaner reaction was observed when CuBr and CuCN were used as catalysts (entries 6 and 7). Under CuBr catalysis, a mixture of **13**, **15** and **17** was obtained in a ratio of 41 : 38 : 21. However, the conversion of **13** decreased to 41%. In contrast, the reaction catalysed by CuCN afforded compound **13** in a conversion of 50%. Even though this conversion was slightly lower than that observed in entry 4, we decided to use this catalyst for the next optimization steps due to the reduced number of by-products formed. The change of the ligand to isopropanol resulted in the formation of only **13** and **15** in a ratio 53 : 47 (entry 8). Decreasing the loading of the catalyst to 10 mol% provided an increase of 10% in the yield (entry 9). Similar results were obtained when 5 mol% of CuCN was used (entry 10). The reactions carried out in the absence of a ligand or using bulkier *tert*-butanol as the ligand gave lower yields (entries 11 and 12). The performance of Cu₂O as the catalyst was similar to that of CuCN furnishing **13** in a conversion of 64% (entry 13). Thus, the best results were achieved using CuOAc (10 mol%) as the catalyst in the presence of K₃PO₄ (3 equiv.) and isopropanol (3 equiv.) at 90 °C for *ca.* 3 days (entry 14, Scheme 2). In this way, the *ortho*-aminated product **13** was obtained in 72% crude yield and 30% isolated yield after the purification steps. The decrease in the yield can be due to the two flash column chromatography eluents needed (eluents: EtOAc:hex 1:1 and subsequently CH₂Cl₂:Et₂O 9:1) in order to isolate the pure compound. As far as we know, there are no precedents about C–N bond-forming reactions of the ATEMPO radical *via* cross-coupling processes.

Extension of the methodology to P-stereogenic phosphinic amides

With the optimized reaction conditions in hand, the application of the methodology to the P-stereogenic phosphinic



Scheme 2 Synthesis of **10** and complexation with Cu(hfac)₂ to give **19**.

amide (*S,S*)-**9a** (dr 94 : 6) afforded compound **10** in 50% crude yield (20% isolated yield).³² The decrease in the yield, compared with that of the achiral analogue **13**, can be attributed to the greater steric encumbrance of the (*S*)-(-)-3,3-dimethyl-2-butylamino moiety of **9a** compared to the isopropyl group present in compound **11**, which probably hinders the approach of 4-amino-TEMPO to the *ortho* position of **9a**. To the best of our knowledge, compound **10** is the first example of a P-stereogenic TEMPO-based radical. The structure of **10** was confirmed by X-ray diffraction of single crystals obtained from the slow evaporation of a solution of the ligand in CHCl₃.

The reaction of (*S_P,S_C*)-**10** with an equimolar amount of Cu(hfac)₂ in a mixture of *n*-heptane/CHCl₃ as the solvent afforded after 30 days at –20 °C dark-green single crystals of **19** in a yield of 20% (Scheme 2). The X-ray diffraction study of the structure showed that the metal ion is coordinated to the oxygen atoms of the phosphinic amide and the TEMPO moieties. As far as we know, there are no precedents for this type of P-stereogenic complex in the literature.

Crystal structural description of 10

Compound **10** crystallizes in the orthorhombic *P*2₁2₁2₁ chiral space group and its molecular structure is shown in Fig. 2. A summary of data collection and refinement is given in Table S1,† while the selected bond lengths and angles are listed in Table 2. The thermal ellipsoids are shown in Fig. S20.†

The molecular structure of compound **10** consists of a neutral 4-substituted amino-TEMPO radical. The N2 atom connects the six-membered TEMPO ring to the chiral P-containing moiety. Starting from the P-containing moiety, the P=O bond length is 1.490(1) Å, which is in the typical distance range of Ph₂P(O)NHR molecules³³ and is in good agreement with the literature values for similar compounds.³⁴ The geometry around the phosphorus atom can be described as a distorted tetrahedron with bond angles ranging from 102.0(1) to 119.0(1)°.

The largest bond angle around the phosphorus atom was observed for the O2–P1–N3 set, and this remarkable structural difference with respect to the other bond angles involving the P atom can be related to the steric hindrance of the 3,3-dimethyl-2-butylamino group. Concerning the P1 and C22 chiral atoms, since the stereogenic centers of the starting phosphinic amide **9a** remained unchanged, both showed the

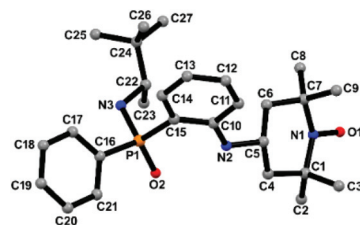


Fig. 2 Representation of the molecular unit of compound **10**. Hydrogen atoms were omitted for clarity. Color codes: Gray: carbon; red: oxygen; orange: phosphorus and blue: nitrogen.

Table 2 Selected bond lengths and angles for **10** and **19**

| Atom labels | (10) | (19) |
|--------------------------------------|----------|-----------|
| N1–O1 | 1.285(2) | 1.292(4) |
| P1–O2 | 1.492(2) | 1.500(2) |
| P1–N3 | 1.649(2) | 1.639(3) |
| P1–C15 | 1.805(2) | 1.799(3) |
| P1–C16 | 1.806(2) | 1.808(3) |
| N2–C5 | 1.451(3) | 1.451(4) |
| N2–C10 | 1.375(3) | 1.383(4) |
| N3–C22 | 1.485(2) | 1.483(4) |
| Cu1–O1 ⁱ | — | 2.569(3) |
| Cu1–O2 | — | 2.224(2) |
| Cu1–O3 | — | 1.960(2) |
| Cu1–O4 | — | 1.955(2) |
| Cu1–O5 | — | 1.952(2) |
| Cu1–O6 | — | 1.958(2) |
| C5–N2–C10 | 123.9(2) | 123.2(3) |
| P1–N3–C22 | 118.0(1) | 123.9(2) |
| O2–P1–C15 | 110.9(1) | 111.0(1) |
| O2–P1–C16 | 110.4(1) | 109.0(1) |
| O2–P1–N3 | 119.0(1) | 118.5(1) |
| N3–P1–C15 | 104.1(1) | 105.1(1) |
| N3–P1–C16 | 102.0(1) | 102.7(1) |
| C15–P1–C16 | 109.8(1) | 109.9(1) |
| Cu1–O2–P1 | — | 150.8(1) |
| Cu1 ⁱ –O1–N1 | — | 158.6(2) |
| Cu1 ⁱ ...Cu1 ⁱ | — | 9.3978(7) |

Symmetry operation: (i) = $-x, 1/2 + y, 1/2 - z$.

expected *S* configuration. The absolute crystal structure was confirmed by the Flack parameter close to zero [0.024(9)].

In the TEMPO radical moiety, the six-membered ring is in the chair conformation with an N–O[•] bond length of 1.285(2) Å, which is similar to those observed in other TEMPO derivatives.²² The plane passing by the TEMPO ring atoms (C1–C5, N1, N2 and O1) is 59.7° displaced from the central phenyl ring (C10–C15 atoms), while the P-phenyl ring is more parallel to the TEMPO one, with an angle of 14.0°. This configuration adopted by the rings is driven by the intramolecular hydrogen bond found in the fragment P=O...HN_{TEMPO} as depicted in Fig. 3. The following geometric parameters were observed for this intramolecular interaction: N2–H2 = 0.88(3) Å, H2...O2 = 1.97(3) Å, N2...O2 = 2.747(2) Å and ∠N2–H2...O2 = 147(2)°.

An intermolecular hydrogen bond involving the TEMPO oxygen atom and α-amino group of the phosphinic amide

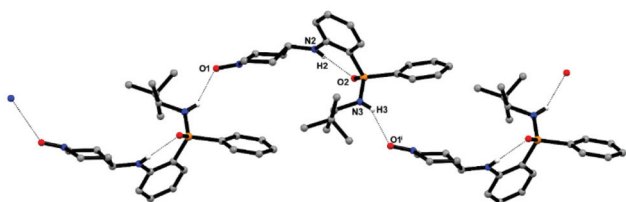


Fig. 3 Details of the crystal packing of **10** showing the intramolecular P=O...HN_{TEMPO} hydrogen bond, and the intermolecular interactions that lead to the formation of a zig-zag supramolecular chain running along the *b* axis. Only the hydrogen atoms involved are shown. Symmetry operation to generate equivalent atoms: (i) = $-x + 3/2, -y + 2, z + 1/2$.

moiety (N3–H3 = 0.87(3) Å, H3...O1ⁱ = 2.12(3) Å, N3...O1ⁱ = 2.988(2) Å; ∠N3H3...O1ⁱ = 173(2)°; *i* = $-x + 3/2, -y + 2, z + 1/2$) gives rise to a zig-zag supramolecular chain running along the *b* axis, as shown in Fig. 3. Each supramolecular chain is connected to the neighbouring ones through P=O...H–C_{sp²} short contacts involving the phosphinic and amino-phenyl groups. The intrachain distance between the paramagnetic sites is 10.423(2) Å. The closest separation among them is 8.379(2) Å, found for the interchain N–O...O–N distance.

Structural description of copper complex (S_P,S_C)-19

Complex (S_P,S_C)-**19** crystallizes in the chiral orthorhombic *P*₂₁₂₁ space group and its crystallographic data and refinement parameters are listed in Table S1.† The thermal ellipsoids of the asymmetric unit are depicted in Fig. S21.† The asymmetric unit consisted of one radical molecule **10** coordinated to a Cu(hfac)₂ moiety by a phosphinic oxygen atom, and one toluene as the lattice solvent. Radical **10** acts as a spacer and leads to the formation of a 1D chiral helical chain running along the *b* axis (Fig. 4). The copper(II) ion shows a tetragonally distorted octahedral geometry, coordinated to four hfac oxygen atoms and two units of the radical ligand through P=O and N–O[•] groups in a *trans* arrangement. The equatorial plane is formed by four hfac oxygen atoms (O3–O6) displaying an average Cu–O distance of 1.956(2) Å, typical of other Cu(hfac)₂ complexes reported elsewhere.³⁵ The axial positions are occupied by two radical molecules, with one oxygen atom from the TEMPO moiety (O1) and the other being the phosphinic oxygen atom (O2). Due to the Jahn–Teller effect, the axial bond lengths are remarkably longer with Cu1–O1ⁱ and Cu–O2 distances of 2.569(3) Å and 2.224(2) Å, respectively. The bond angle involving the copper ion and the TEMPO moiety (Cu1ⁱ–O1–N1, *i* = $-x, 1/2 + y, 1/2 - z$) is 158.6(2)°. In addition, the bond angles between the atom from the equatorial plane and apical positions are in the range of 83.13(9)° (O6–Cu1–O1) to 101.42(9)° (O2–Cu1–O5), while the largest

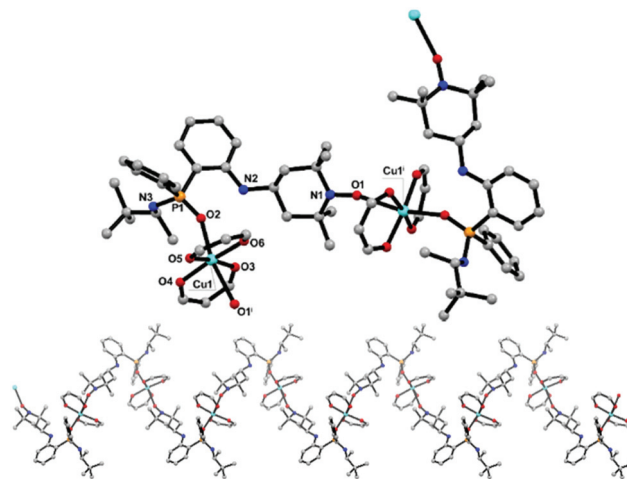


Fig. 4 Fragment of the helicate chain of (S_P,S_C)-**19** with atom numbering (top). A 1D chain running parallel to the *b* crystallographic axis (S_P,S_C)-**19**. Hydrogen and CF₃ groups were omitted for clarity.

deviation from an ideal octahedral geometry is $168.05(8)^\circ$, found for the apical positions (O1–Cu1–O2).

The shortest intrachain distance between the copper(II) ion is $9.3978(7)$ Å (Cu1...Cu1ⁱ, $i = -x, 1/2 + y, 1/2 - z$), whereas the shortest intermolecular one is $12.0437(7)$ Å (Cu1...Cu1ⁱⁱ, $ii = 1 - x, -1/2 + y, 3/2 - z$). Since the direct coordination among copper and the nitroxide moiety of **10** was achieved, the shortest intramolecular distance found between the paramagnetic sites is indeed $2.569(2)$ Å, which is slightly longer than those observed in other complexes with Cu–ON and an octahedral geometry around the metal described to date (in the range of 2.33 – 2.52 Å).³⁶ As observed in the crystal structure of **10**, an intramolecular hydrogen bond in between the P=O...HN_{TEMPO} fragment is also present in **19**, with the following geometric parameters: N2–H2 = $0.80(4)$ Å, H2...O2 = $2.07(4)$ Å, N2...O2 = $2.785(4)$ Å and \angle N2–H2...O2 = $149(4)^\circ$. This intramolecular interaction acts as the driving force to maintain the same radical conformation in **19**, as seen in pro-ligand **10**.

The crystal packing is stabilized by a network of hydrogen bonds involving C_{sp3}H...F from hfac and methyl groups from the TEMPO units, and C_{sp2}H...F between hfac and the phenyl ring. Moreover, weak interactions, namely C_{sp3}H...C_{sp2} and C_{sp2}H...C_{sp2}, are also found among the toluene crystallization molecules and the chain, which are responsible for the intermolecular stabilization between the 1D polymeric helices.

Magnetic properties of 10

Fig. 5 shows the thermal dependence of the $\chi_M T$ product for **10** (χ_M is the molar magnetic susceptibility). At room temperature, the $\chi_M T$ value is 0.377 cm³ mol⁻¹ K as expected for a magnetically isolated spin doublet, $S = 1/2$. Upon cooling, $\chi_M T$ remains basically constant until ca. 10 K, and then it decreases to ca. 0.335 cm³ mol⁻¹ K at 2.0 K. No maximum of the magnetic susceptibility is observed above 2 K. These features are characteristic of the occurrence of very weak intermolecular antiferromagnetic interactions. The observed data were analyzed on the basis of eqn (1), where N , β , k and g have their usual meanings, θ is the Weiss parameter and $S = \frac{1}{2}$.

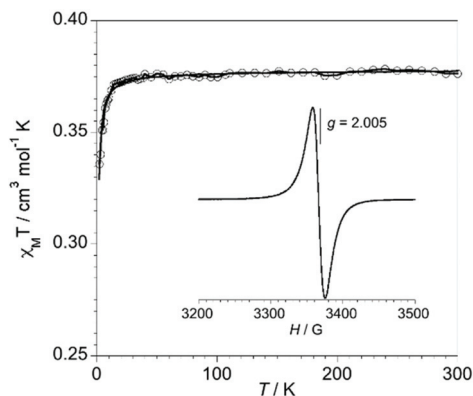


Fig. 5 $\chi_M T$ vs. T plot of complex **10**. The circles represent the experimental results and the solid line represents the best-fit curve through eqn (1). The inset shows the X-Band EPR spectrum of **10** at 4.3 K.

The best fit of the magnetic data was $g = 2.00(1)$ and $\theta = -0.290(2)$ K. The theoretical curve and the experimental data match quite well over the entire temperature range, as depicted in Fig. 5. The X-band EPR spectrum of **10** in the solid state (see the inset of Fig. 5) shows a narrow signal centered at 2.005, which is characteristic of free radicals.³⁷

$$\chi_M = \frac{N\beta^2 g^2}{k(T - \theta)} S(S + 1). \quad (1)$$

Magnetic properties of 19

Fig. 6 shows the thermal dependence of the $\chi_M T$ product for **19** (χ_M is the magnetic susceptibility per Cu(II) ion and per radical). At room temperature, the $\chi_M T$ value is 0.79 cm³ mol⁻¹ K as expected for two spin doublets magnetically isolated (one Cu(II) ion and one radical). Upon cooling, the $\chi_M T$ values continuously increase and attain a maximum value of 0.98 cm³ mol⁻¹ K at 5.0 K, and then decrease rapidly. In the high temperature region, the shape of this curve is indicative of the occurrence of a ferromagnetic interaction between both paramagnetic centers (Cu–radical), while the decrease at low temperature could be the result of the presence of antiferromagnetic interactions and/or zero-field splitting (zfs) effects. However, due to the low anisotropy of this complex, the important zfs effect is not expected.

Having in mind the 1D polymeric topology of **19**, where the radical acts as a bridging ligand through its oxygen–nitroxide and oxygen–phosphinic donor atoms, the spin magnetic coupling pattern can be summarized in Scheme 3.

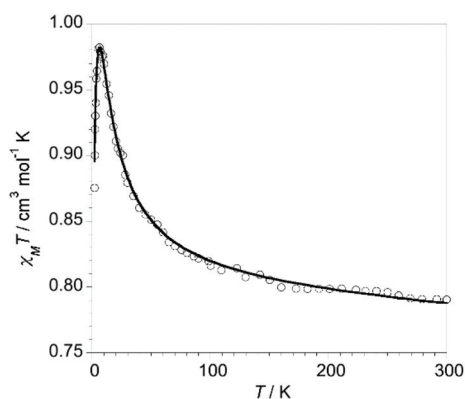
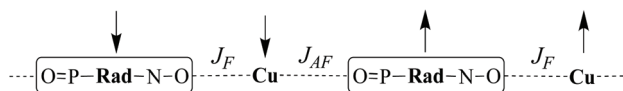


Fig. 6 $\chi_M T$ vs. T plot of complex **19**. The circles represent the experimental results and the solid line represents the best-fit curve through eqn (2).



Scheme 3 Model of the magnetic interactions of **19** applied to fit the data.

Given the occurrence of both ferro- and antiferromagnetic interactions in **19** and the presence of two different magnetic exchange pathways, we analyze the magnetic data through a numerical expression for an alternating ferro- and antiferromagnetic Heisenberg chain derived by Georges *et al.*³⁸ The corresponding Hamiltonian is defined using eqn (2), where J is the exchange coupling parameter associated with a particular copper(II)-radical pair and αJ is the exchange constant assigned to the adjacent unit (the alternating parameter α is defined as the $J_F/|J_{AF}|$ quotient).

$$\hat{H} = -J \sum_{i=1}^{n/2} (\hat{S}_{2i} \hat{S}_{2i-1} - \alpha \hat{S}_{2i} \hat{S}_{2i+1}). \quad (2)$$

Least-squares best-fit parameters obtained were $J = 12.6(1) \text{ cm}^{-1}$, $\alpha J = 1.11(1) \text{ cm}^{-1}$, and $g = 2.11(1)$, where g is the average value of g_{Cu} and g_{rad} . Due to the unpaired electron of the radical which is localized on an N-TEMPO π -orbital, the strongest magnetic interaction can be attributed to the Rad-N-O-Cu pathway, $J_F = +12.1 \text{ cm}^{-1}$, while the weakest one must be attributed to the longest phosphinic amide magnetic pathway, $J_{AF} = -1.11 \text{ cm}^{-1}$. These relatively small values can be understood by looking at the relative disposition of the magnetic orbitals involved. In both intrachain pathways, the magnetic orbital at each copper(II) site (that is the molecular orbital describing the unpaired electron) is of the $d(x^2-y^2)$ -type and it is mainly delocalized on the equatorial plane (the plane formed by the hfac ligands) and so, the spin density at the apical position is predicted to be very small.

The Cu(II)- $d(x^2-y^2)$ magnetic-orbital and the O-(nitroxide) π -orbital are orthogonal, leading to a ferromagnetic interaction.³⁹ The small value of this ferromagnetic interaction is due to the long bond distance Cu-O(1) (2.57 Å) as a consequence of the Jahn-Teller effect. Similar ferromagnetic interactions were observed in other Cu(II)-TEMPO systems.⁴⁰

The magnetic interaction Cu(II)-TEMPO through the phosphinic amide substituent is expected to be very small, if any. So, the calculated value $J_{AF} = -1.11 \text{ cm}^{-1}$ seems to be too large and, although the chains are quite magnetically isolated within the crystal, some interchain antiferromagnetic interactions could be present. In fact, the magnetic data can be reproduced by ruling out this magnetic interaction and using the Bleaney-Bowers equation (eqn (2)), which describes the magnetic interaction between the two spin doublets, and introducing a Weiss parameter, θ , to take into account the intermolecular interactions. The best-fit parameters obtained through eqn (2) were $J = +12.6(1) \text{ cm}^{-1}$, $g = 2.11(1)$ and $\theta = -0.365(3) \text{ K}$. In this sense, the value of $J_{AF} = -1.11 \text{ cm}^{-1}$ obtained for the magnetic interaction Cu(II)-TEMPO through the phosphinic group would be the upper limit for this magnetic interaction.

Conclusions

In summary, we have shown the feasibility of introducing a 4-amino-TEMPO radical at the *ortho* position of *ortho*-iodopho-

sphinic amides *via* Cu(I) catalyzed cross-coupling reactions. Conversions of 50 to 72% were achieved using CuOAc (10 mol%) as the catalyst (isolated yields of 20 to 30%). This methodology was applied to the synthesis of a P-stereogenic phosphinic amide-*ortho*-ATEMPO radical. Its coordination behavior with Cu(hfac)₂ provided a P-stereogenic complex with a polymeric helicate chain built by the coordination of the oxygen atoms of the phosphinic amide and nitroxide donor sites to the Cu(II) ions. To the best of our knowledge, these are the first examples of C_{sp²}-N cross-coupling reactions of ATEMPO and of a P-stereogenic-*ortho*-ATEMPO radical and its copper(II) complex. The magnetic properties of the chiral compounds showed very weak intermolecular antiferromagnetic interactions for the ligand, while ferro- and anti-ferromagnetic interactions were observed for the copper(II) complex. The extension of the application of the novel chiral P-stereogenic ATEMPO-based radical in catalysis and coordination chemistry is underway.

Experimental section

Instrumentation and reagents

All reactions and manipulations were carried out under a dry N₂ gas atmosphere using standard Schlenk procedures. THF was distilled from sodium/benzophenone immediately prior to use. Commercial reagents were distilled prior to their use, except for *tert*-butyllithium and chiral amine. TLC was performed on Merck plates with aluminium backing and silica gel 60. Purification was carried out by column chromatography using silica gel 60 (40–63 μm) from Scharlau and different mixtures of ethyl acetate : hexane and methylene chloride : diethyl ether as the eluent. NMR spectra were recorded on a Bruker Avance 300 (¹H, 300.13 MHz; ¹³C, 75.47 MHz; and ³¹P, 121.49 MHz). The spectral references used were tetramethylsilane as the internal standard for ¹H and ¹³C spectroscopy, and 85% H₃PO₄ as the external standard for ³¹P spectroscopy. Diastereoselectivities were determined by the integration of the ³¹P NMR spectra of the crude reaction mixtures. The standard Bruker software was used for acquisition and processing methods. Infrared spectra were recorded using Bruker Alpha FTIR equipment. High resolution mass spectra were recorded on Agilent Technologies LC/MSD TOF and HP 1100 MSD equipment with electrospray ionization. Melting points were recorded using Büchi B-540 capillary melting point apparatus and are uncorrected. Compounds **9a** and **11** were prepared according to a method described in the literature.²⁶

X-ray diffraction

Crystallographic data were collected using a Bruker APEX II CCD area detector at 100 K, using CuK α radiation ($\lambda = 1.54178 \text{ \AA}$). Data collection and cell refinement were performed with Bruker APEX2⁴¹ and Bruker SAINT,⁴² respectively. Data reduction was done using SAINT. Empirical multiscan absorption correction using equivalent reflections was performed using the SADABS program.⁴³ The structure solution and full-

matrix least-squares refinements based on F^2 were performed using SHELXS⁴⁴ and SHELXL⁴⁵ programs, respectively. All atoms except hydrogen were refined anisotropically. The structures were drawn using the Mercury program.⁴⁶

Magnetic measurements

Variable-temperature (2–300 K) direct current (dc) magnetic susceptibility measurements on the crushed crystals of **10** and **19** under an applied field of 0.1 T were carried out with a Quantum Design SQUID magnetometer. The data were corrected for the diamagnetism of the constituent atoms and the sample holder. The X-band EPR spectra of the powdered samples were recorded at 4.3 K using a Bruker ER 200 spectrometer equipped with a helium cryostat.

Synthesis of the compounds

General procedure for the preparation of 9a and 11. Compounds **9a** and **11** were prepared according to a method described in the literature.²⁶ To a solution of the corresponding phosphinic amide (3.3 mmol) in 10 mL of THF, *t*-BuLi (2.2 equiv. of a 1.7 M solution in pentane) was added at –78 °C. After 1 hour of stirring, 1.2 equiv. of 1,2-diiodoethane were added and the reaction was allowed to reach room temperature for an additional 15 minutes. Then, the mixture was poured into water, extracted with ethyl acetate (3 × 20 mL), and dried with anhydrous Na₂SO₄ and the solvents were removed using a Rotavapor system. Purification: flash column chromatography (EtOAc : hex 4 : 1 as the eluent).

(S)-N-((S)-3,3-Dimethylbutan-2-yl)-P-(2-iodophenyl)-P-phenylphosphinic amide (9a). The characterization of this compound is described.²⁶ Yield: 80%. [α]_D²⁵ +148.1 (c 0.9, CH₂Cl₂). The NMR data obtained are in excellent agreement with those reported in the literature. ¹H NMR (CDCl₃) δ 8.29 (ddd, 1H, ³J_{PH} 12.1, ³J_{HH} 7.6, ⁴J_{HH} 1.7 Hz), 7.90 (dd, 1H, ³J_{HH} 7.9, ⁴J_{PH} 3.8 Hz), 7.64 (dd, 2H, ³J_{PH} 13.1, ³J_{HH} 6.9 Hz), 7.40 (m, 2H), 7.49 (m, 2H), 7.15 (t, 1H, ³J_{HH} 7.6 Hz), 3.41 (ddc, 1H, ³J_{PH} 19.7, ³J_{HH} 10.1, ³J_{HH} 6.6 Hz), 3.24 (dd, 1H, ²J_{PH} 14.3, ³J_{HH} 10.3 Hz), 1.30 (d, 3H, ³J_{HH} 6.6 Hz), 0.80 (s, 9H) ppm. ³¹P{¹H} NMR (CDCl₃) δ 26.6 (s) ppm.

N-Isopropyl-P-(2-iodophenyl)-P-phenylphosphinamide (11). Yield: 72%. White solid. Mp: 108–109 °C. ¹H NMR (CDCl₃) δ 8.29 (ddd, 1H, ³J_{PH} 12.5, ³J_{HH} 7.6, ⁴J_{HH} 1.6 Hz), 7.98 (ddd, 1H, ³J_{HH} 8.0, ⁴J_{PH} 3.9, ⁴J_{HH} 1.3 Hz), 7.77 (ddd, 2H, ³J_{PH} 12.7, ³J_{HH} 8.0, ⁴J_{HH} 1.3 Hz), 7.49 (m, 2H), 7.51 (m, 2H), 7.18 (tt, 1H, ³J_{HH} 7.8, ⁴J_{HH} 1.3 Hz), 3.62 (m, 1H), 3.17 (t, 1H, ²J_{PH} = ³J_{HH} 10.3 Hz), 1.32 (d, 3H, ³J_{HH} 6.5 Hz), 1.20 (d, 3H, ³J_{HH} 6.5 Hz) ppm. ¹³C{¹H} NMR (CDCl₃) δ 141.5 (d, ²J_{PC} 9.5 Hz), 136.6 (d, ¹J_{PC} 125.5 Hz), 136.1 (d, ³J_{PC} 8.4 Hz), 132.9 (d, ⁴J_{PC} 2.8 Hz), 132.1 (d, ²J_{PC} 9.6 Hz), 132.0 (d, ⁴J_{PC} 3.6 Hz), 131.9 (d, ¹J_{PC} 131.9 Hz), 128.5 (d, ³J_{PC} 13.7 Hz), 127.8 (d, ³J_{PC} 10.2 Hz), 98.8 (d, ²J_{PC} 7.3 Hz), 43.5 (d, ²J_{PC} 1.4 Hz), 26.2 (d, ³J_{PC} 5.4 Hz), 25.4 (d, ³J_{PC} 4.9 Hz) ppm. ³¹P{¹H} NMR (CDCl₃) δ 25.9 (s) ppm. IR (KBr): ν 3250 (bs), 2967 (s), 1422 (s), 1198 (s, P=O), 1114 (s), 730 (s), 690 (m) cm⁻¹. HRMS (ESI) calcd for C₁₅H₁₇NOPI: 386.0171, found: 386.0177.

The optimized conditions for the synthesis of phosphinic amide-TEMPO ligands. To a dry Schlenk, *ortho*-iodophosphinic amide (0.1 mmol, 1 equiv.), K₃PO₄ (0.3 mmol, 3 equiv.) and CuOAc (10 mol%) were added and dried *in vacuo* for 15 min. Then, 4-amino-TEMPO (10 equiv.) and isopropanol (0.3 mmol, 3 equiv.) were added under a dry atmosphere and the mixture was warmed to 90 °C and stirred for *ca.* 3 days. After this time, the reaction mixture was diluted with ethyl acetate, filtered through Celite and poured into water. Then, the crude mixture was extracted with EtOAc (3 × 15 mL), and dried with Na₂SO₄ and the solvents were removed under reduced pressure. For the purification of the compounds, two flash column chromatography eluent mixtures were needed: for the first one, EtOAc:hex 1:1 was used as the eluent mixture, and CH₂Cl₂:Et₂O 9:1 was used as the eluent mixture for the second one.

N-Isopropyl-P-(2-((1-oxyl-2,2,6,6-tetramethylpiperidin-4-yl)amino)phenyl)-P-phenylphosphinic amide (13). Yield: 30%. Red solid. Mp: 76–77 °C. ¹H NMR (CDCl₃) δ 7.92 (bs, 2H), 7.55 (bs, 5H), 7.40 (bs, 1H), 6.78 (bs, 1H), 3.54 (bs, 1H), 2.76 (bs, 1H), 1.35 (bs, 12H) ppm. ³¹P{¹H} NMR (CDCl₃) δ 29.6 (s) ppm. IR (KBr): ν 3345 (bs), 2971 (s), 2932 (s) 1596 (s), 1455 (s), 1242 (s), 1175 (s, P=O), 750 (m), 696 (w) cm⁻¹. HRMS (ESI) calcd for C₂₄H₃₆N₃O₂P: 429.2545, found: 429.2604. The structural assignment was confirmed by adding an equimolecular amount of phenyl hydrazine to the NMR sample to give *N*-isopropyl-P-(2-((1-hydroxy-2,2,6,6-tetramethylpiperidin-4-yl)amino)phenyl)-P-phenylphosphinic amide. Yield: 100%. ¹H NMR (CDCl₃) δ 7.87 (ddt, 2H, ³J_{PH} 11.9, ³J_{HH} 7.9 Hz, ⁴J_{HH} 1.5 Hz), 7.41–7.55 (m, 5H), 6.63 (m, 2H), 3.45 (m, 1H), 2.77 (dd, 1H, ²J_{PH} 9.9, ³J_{HH} 6.3 Hz), 2.09 (dt, 1H, ¹J_{HH} 13.0 Hz, ³J_{HH} 3.5 Hz), 1.96 (dt, ¹J_{HH} 13.2 Hz, ³J_{HH} 3.4 Hz, 1H), 1.58 (m, 1H), 1.28 (m, 18H) ppm. ³¹P NMR (CDCl₃) δ 29.4 (s) ppm. HRMS (ESI) calcd for C₂₄H₃₇N₃O₂P: 430.2623, found: 430.2702.

(S_P)-N-((S_C)-3,3-Dimethylbutan-2-yl)-P-(2-((1-oxyl-2,2,6,6-tetramethylpiperidin-4-yl)amino)phenyl)-P-phenylphosphinic amide (10). Yield: 20%. Red solid. Mp: 175–176 °C. [α]_D²⁵ +395.9 (c 0.45, CH₂Cl₂). ¹H NMR (CDCl₃) δ 7.95 (bs, 2H), 7.41 (bs, 4H), 7.37 (bs, 1H), 6.73 (bs, 1H), 3.00 (bs, 1H), 2.76 (bs, 1H), 2.42 (bs, 2H), 1.55 (bs, 4H), 1.32 (bs, 15H), 0.98 (bs, 9H) ppm. ³¹P{¹H} NMR (121.49 MHz, CDCl₃) δ 30.0 (s) ppm. IR (KBr): ν 3256 (bs), 2961 (s), 1586 (s), 1457 (s), 1241 (s), 1172 (s, P=O), 1114 (s), 747 (m), 699 (m) cm⁻¹. HRMS (ESI) calcd for C₂₇H₄₂N₃O₂P: 471.3009, found: 471.3019. The structural assignment was confirmed by adding an equimolecular amount of phenyl hydrazine to the NMR sample to reduce the radical. Yield: 100%. ¹H NMR (CDCl₃) δ 7.92 (ddd, 2H, ³J_{PH} 11.6, ³J_{HH} 7.6, ⁴J_{HH} 1.6 Hz), 7.48 (m, 5H), 6.63 (m, 2H), 3.70 (m, 1H), 3.00 (m, 1H), 2.76 (dd, ²J_{PH} 11.1, ³J_{HH} 5.3 Hz), 2.08 (dt, 1H, ²J_{HH} 13.0, ³J_{HH} 3.6 Hz), 1.99 (dt, 1H, ²J_{HH} 13.1, ³J_{HH} 3.6 Hz), 1.58 (m, 2H), 0.93 (s, 9H), 1.28 (m, 15H) ppm. ³¹P NMR (CDCl₃) δ 30.3 (s) ppm. HRMS (ESI) calcd for C₂₇H₄₃N₃O₂P: 472.3087, found: 472.3097.

Synthesis of the copper complex (19). 0.021 mmol of Cu(hfac)₂·2H₂O was added to 10 mL of boiling *n*-heptane. When the metal complex was completely dissolved, 0.021 mmol of

the chiral 4-amino-TEMPO ligand dissolved in CHCl_3 was quickly added under constant stirring. The solution was boiled for 5 minutes and then allowed to cool. Green crystals suitable for X-ray diffraction analysis were obtained after 30 days at $-18\text{ }^\circ\text{C}$. Yield: 20%. Mp: 127–128 $^\circ\text{C}$. $[\alpha]_{\text{D}}^{25} +508.5$ (c 0.2, CH_2Cl_2). IR (ATR, cm^{-1}): 3319 (w, NH), 1645 (s, CO), 1259 (s, CF), 1211 (s), 1149 (s, P=O), 797 (m), 679 (m). Anal. calc. for $\text{C}_{37}\text{H}_{43}\text{CuF}_{12}\text{N}_3\text{O}_6\text{P}$: C, 46.87%; H, 4.43%; N, 4.57%. Found: C, 46.54%; H, 4.81%; N, 4.24%. Although the crystal structure of the complex shows one toluene molecule as the lattice solvent, the elemental analysis result is more consistent with the toluene-free formula, suggesting the ready loss of this solvent molecule during microanalysis.

By-products obtained during the optimization procedure

***N*-Isopropyl-*P*-(2-butoxyphenyl)-*P*-phenylphosphinic amide (14).** Obtained through flash column chromatography (EtOAc:hex 1:1 as the eluent mixture) from the reaction in entry 3 (Table 1, main text). Yield: 40%. Colorless oil. ^1H NMR (CDCl_3) δ 7.86 (m, 3H), 7.47 (m, 4H), 7.05 (ddt, 1H, $^3J_{\text{HH}}$ 7.4, $^4J_{\text{PH}}$ 2.0, $^4J_{\text{HH}}$ 0.9 Hz), 6.87 (ddd, 1H, $^3J_{\text{HH}}$ 8.3, $^4J_{\text{PH}}$ 5.3, $^4J_{\text{HH}}$ 0.8 Hz), 4.00 (m, 2H), 3.56 (m, 1H), 3.39 (t, 1H, $^3J_{\text{HH}}$ 8.7 Hz), 1.69 (m, 2H), 1.43 (m, 2H), 1.20 (d, $^3J_{\text{HH}}$ 6.3 Hz, 3H), 1.19 (dd, 3H, $^3J_{\text{HH}}$ 6.3 Hz, $^4J_{\text{PH}}$ 0.5 Hz), 0.96 (t, 3H, $^3J_{\text{HH}}$, 6.3 Hz) ppm. ^{13}C $\{^1\text{H}\}$ NMR (CDCl_3) δ 159.3 (d, $^2J_{\text{PC}}$ 3.6 Hz), 135.4 (d, $^1J_{\text{PC}}$ 131.7 Hz), 134.3 (d, $^2J_{\text{PC}}$ 7.5 Hz), 133.3 (d, $^4J_{\text{PC}}$ 2.5 Hz), 131.8 (d, $^2J_{\text{PC}}$ 10.6 Hz), 128.2 (d, $^3J_{\text{PC}}$ 12.2 Hz), 131.3 (d, $^4J_{\text{PC}}$ 3.5 Hz), 121.6 (d, $^1J_{\text{PC}}$ 124.4 Hz), 121.0 (d, $^3J_{\text{PC}}$ 11.6 Hz), 111.5 (d, $^3J_{\text{PC}}$ 7.2 Hz), 68.3 (d, $^3J_{\text{PC}}$ 0.3 Hz), 42.6 (d, $^2J_{\text{PC}}$ 1.5 Hz), 30.0 (s), 26.2 (d, $^3J_{\text{PC}}$ 3.4 Hz), 26.0 (d, $^3J_{\text{PC}}$ 7.0 Hz), 19.8 (s), 13.9 (s) ppm. $^{31}\text{P}\{^1\text{H}\}$ NMR (CDCl_3) δ 23.9 (s) ppm. IR (solid film): 3444 (bs), 2961 (m), 1590 (m), 1440 (m), 1278 (w), 1195 (bs, P=O), 1135 (w), 757 (m), 696 (m). HRMS (ESI) calcd for $\text{C}_{19}\text{H}_{27}\text{NO}_2\text{P}$: 332.1779, found: 332.1778.

***N*-Isopropyl-*P*,*P*-diphenylphosphinic amide (15).** Obtained through flash column chromatography (EtOAc:hex 1:1 as the eluent mixture) from the reaction in entry 4 (Table 1, main text). Yield: 8%. White solid. The NMR data obtained for the compound are in agreement with those reported in the literature.⁴⁷ ^1H NMR (CDCl_3) δ 7.93 (m, 4H), 7.49 (m, 6H), 3.40 (sep, $^3J_{\text{HH}}$ 6.6 Hz), 2.70 (t, 1H, $^3J_{\text{HH}}$ 7.5 Hz), 1.26 (d, 6H, $^3J_{\text{HH}}$ 6.6 Hz) ppm. $^{31}\text{P}\{^1\text{H}\}$ NMR (CDCl_3) δ 22.8 (s) ppm.

***N*-Isopropyl-*P*-(2-hydroxyphenyl)-*P*-phenylphosphinic amide (16).** White solid. Only traces of the compound were obtained from the crude reaction mixture in entry 4 (Table 1, main text), *via* flash column chromatography (EtOAc:hex 1:1 as the eluent mixture). The assignment of the structure was carried out based on the ^1H and $^{31}\text{P}\{^1\text{H}\}$ NMR spectra and through comparison with the corresponding spectra of a chiral analogue described in the literature.²⁶ ^1H NMR (CDCl_3) δ 11.61 (s, 1H), 7.94 (dd, 2H, $^3J_{\text{PH}}$ 10.7, $^3J_{\text{HH}}$ 6.8 Hz), 7.50 (m, 4H), 7.40 (m, 1H), 6.92 (m, 2H), 3.46 (m, 1H), 2.91 (m, 1H), 1.33 (d, 3H, $^3J_{\text{HH}}$ 6.5 Hz), 1.25 (d, 3H, $^3J_{\text{HH}}$ 6.5 Hz) ppm. $^{31}\text{P}\{^1\text{H}\}$ NMR (CDCl_3) δ 31.5 (s) ppm.

***N*-Isopropyl-*P*-(2-(2-hydroxyethoxy)phenyl)-*P*-phenylphosphinic amide (17).** Obtained from the crude reaction mixture in

entry 4 (Table 1, main text) through flash column chromatography (EtOAc:hex 1:1 as the eluent mixture). Yield: 10%. Colorless oil. ^1H NMR (CDCl_3) δ 7.93 (m, 2H), 7.59 (m, 1H), 7.53 (m, 2H), 1.18 (d, 3H, $^3J_{\text{HH}}$ 6.4 Hz), 7.46 (dddd, 1H, $^3J_{\text{HH}}$ 8.3, $^3J_{\text{HH}}$ 7.4, $^4J_{\text{HH}}$ 1.7, $^5J_{\text{PH}}$ 1.0 Hz), 7.18 (m, 1H), 7.14 (ddd, 1H, $^3J_{\text{PH}}$ 14.0, $^3J_{\text{HH}}$ 7.4, $^4J_{\text{HH}}$ 1.7 Hz), 7.00 (ddd, 2H, $^3J_{\text{HH}}$ 8.3, $^4J_{\text{PH}}$ 5.0, $^4J_{\text{HH}}$ 0.9 Hz), 6.96 (ddt, 1H, $^3J_{\text{HH}}$ 7.4, $^4J_{\text{PH}}$ 2.8, $^4J_{\text{HH}}$ 0.9 Hz), 4.2–4.4 (m, 2H), 3.88 (m, 2H), 3.41 (sep, 1H, $^3J_{\text{HH}}$ 6.4 Hz), 1.33 (d, 3H, $^3J_{\text{HH}}$ 6.4 Hz) ppm. $^{13}\text{C}\{^1\text{H}\}$ NMR (CDCl_3) δ 160.8 (d, $^2J_{\text{PC}}$ 2.0 Hz), 133.5 (d, $^4J_{\text{PC}}$ 2.1 Hz), 133.0 (d, $^2J_{\text{PC}}$ 9.8 Hz), 132.4 (d, $^2J_{\text{PC}}$ 9.3 Hz), 132.1 (d, $^4J_{\text{PC}}$ 2.8 Hz), 131.0 (d, $^1J_{\text{PC}}$ 133.1 Hz), 128.5 (d, $^3J_{\text{PC}}$ 13.1 Hz), 123.5 (d, $^1J_{\text{PC}}$ 129.3 Hz), 121.5 (d, $^3J_{\text{PC}}$ 13.1 Hz), 115.0 (d, $^3J_{\text{PC}}$ 7.0 Hz), 73.3 (s), 61.1 (s), 44.0 (d, $^2J_{\text{PC}}$ 1.9 Hz), 26.4 (d, $^3J_{\text{PC}}$ 3.1 Hz), 25.8 (d, $^3J_{\text{PC}}$ 9.2 Hz) ppm. $^{31}\text{P}\{^1\text{H}\}$ NMR (CDCl_3) δ 28.0 (s) ppm. IR (solid film): 3424 (bs), 2924 (m), 1591 (m), 1441 (m), 1278 (w), 1150 (bs, P=O), 1133 (m), 756 (m), 696 (m) cm^{-1} . HRMS (ESI) calcd for $\text{C}_{17}\text{H}_{23}\text{NO}_3\text{P}$: 320.1416, found: 320.1417.

(*S*)-*N*-(3,3-Dimethylbutan-2-yl)-*P*,*P*-diphenylphosphinic amide (18). Obtained from the crude of the reaction of **9a** with 4-amino-TEMPO. The NMR results are in agreement with those reported in the literature.²⁶ Yield: 29%. ^1H NMR (CDCl_3) δ 7.92 (m, 4H), 7.45 (m, 6H), 2.90 (ddc, 1H, $^3J_{\text{HH}}$ 11.1, $^3J_{\text{PH}}$ 8.7, $^3J_{\text{HH}}$ 6.7 Hz), 2.68 (dd, 1H, $^3J_{\text{HH}}$ 11.1 Hz, $^2J_{\text{PH}}$ 5.2 Hz), 1.21 (d, 3H, $^3J_{\text{HH}}$ 6.7 Hz), 0.90 (s, 9H) ppm. $^{31}\text{P}\{^1\text{H}\}$ NMR (CDCl_3) δ 22.4 (s) ppm.

Conflicts of interest

There are no conflicts to declare.

Acknowledgements

Financial support from Ministerio de Economía y Competitividad (MINECO) and the FEDER program (projects CTQ2014-57157-P, CTQ2016-75671-P, CTQ2016-75068-P, and Excellence Unit “María de Maeztu” MDM-2015-0538) is gratefully acknowledged. GPG acknowledges the financial support from Fundação Carlos Chagas de Amparo à Pesquisa do Estado do Rio de Janeiro – FAPERJ (project number E-26/202.720/2018). YNG thanks Ministerio de Educación, Cultura y Deporte (MECD)^{40a} for a PhD fellowship.

Notes and references

- For recent reviews see: (a) C. Gong and X. Zang, *Science*, 2019, **363**, eaav4450; (b) M. Gobbi, M. A. Novak and E. Del Barco, *J. Appl. Phys.*, 2019, **125**, 240401; (c) L. Guo, X. Gu, X. Zhu and X. Sun, *Adv. Mater.*, 2019, **31**, 1805355; (d) M. Atzori and R. Sessoli, *J. Am. Chem. Soc.*, 2019, **141**, 11339–11352; (e) Z.-S. Yao, Z. Tang and J. Tao, *Chem. Commun.*, 2020, **56**, 2071–2086.
- (a) G. L. J. A. Rikken and E. Raupach, *Nature*, 1997, **390**, 493–494; (b) T. Cyrille, M. Gruselle and M. Verdager, *Chem. Soc. Rev.*, 2001, **40**, 3297–3312; (c) L. Bogani,

- L. Cavigli, K. Bernot, R. Sessoli, M. Gurioli and D. Gatteschi, *J. Mater. Chem.*, 2006, **16**, 2587–2592; (d) R. Sessoli, M. E. Boulon, A. Caneschi, M. Mannini, L. Poggini, F. Wilhelm and A. Rogalev, *Nat. Phys.*, 2015, **11**, 69–74; (e) J. A. Rodriguez-Velamazán, O. Fabelo, J. Campo, J. Rodriguez-Carvajal, N. Qureshi and L. C. Chapon, *Sci. Rep.*, 2018, **8**, 1–7; (f) K. Ishii, S. Hattori and Y. Kitagawa, *Photochem. Photobiol. Sci.*, 2020, **19**, 8–19.
- 3 (a) K. Hemmat, M. A. Nasser and A. Allahresani, *Appl. Organomet. Chem.*, 2019, **33**, e4937; (b) G. Goyal, S. Bhakta and P. Mishra, *ACS Appl. Nano Mater.*, 2019, **2**, 6747–6756.
- 4 (a) A. Caneschi, A. Grand, J. Laugier, P. Rey and R. Subra, *J. Am. Chem. Soc.*, 1988, **110**, 2307–2309; (b) J. Laugier, J. M. Latour, A. Caneschi and P. Rey, *Inorg. Chem.*, 1991, **30**, 4474–4477; (c) I. Ratera and J. Veciana, *Chem. Soc. Rev.*, 2012, **41**, 303–349.
- 5 (a) M. G. Capraro, P. Franchi, O. Lanzalunga, A. Lapi and M. Lucarini, *J. Org. Chem.*, 2014, **79**, 6435–6443; (b) S. Hamada, Y. Wada, T. Sasamori, N. Tokitoh, T. Furura and T. Kawabata, *Tetrahedron Lett.*, 2014, **55**, 1943–1945; (c) M. Carbó-López, P. Y. Chavant, F. Molton, G. Royal and V. Blandin, *ChemistrySelect*, 2017, **2**, 443–450.
- 6 (a) D. B. Amabilino, in *Chirality in Supramolecular Assemblies: Causes and Consequences*, ed. F. R. Keene, John Wiley & Sons, New York, 2017, ch. 6, pp. 159–189; (b) W. Zhai, Y. Feng, H. Liu, A. Rockenbauer, D. Mance, S. Li, Y. Song, M. Baldus and Y. Liu, *Chem. Sci.*, 2018, **9**, 4381–4391.
- 7 (a) Y. Takemoto, T. Yamamoto, N. Ikuma, Y. Uchida, K. Suzuki, S. Shimono, H. Takahashi, N. Sato, Y. Oba, R. Inoue, M. Sugiyama, H. Tsue, T. Kato, J. Yamauchi and R. Tamura, *Soft Matter*, 2015, **11**, 5563–5570; (b) K. Suzuki, Y. Takemoto, S. Takaoka, K. Taguchi, Y. Uchida, D. G. Mazhukin, I. A. Grigor'ev and R. Tamura, *Chem. Commun.*, 2016, **52**, 3935–3938; (c) Y. Takemoto, Y. Uchida, S. Shimono, J. Yamauchi and R. Tamura, *Mol. Cryst. Liq. Cryst.*, 2017, **647**, 279–289; (d) S. Nakagami, T. Akita, D. Kiyohara, Y. Uchida, R. Tamura and N. Nishiyama, *J. Phys. Chem. B*, 2018, **122**, 7409–7415.
- 8 (a) X.-Y. Qin, G.-R. Ding, X.-W. Wang, J. Tan, G.-Z. Guo and X.-L. Sun, *J. Chem. Res.*, 2009, 511–514; (b) T.-Y. Shi, D.-Q. Zhao, H.-B. Wang, S. Feng, S.-B. Liu, J.-H. Xing, Y. Qu, P. Gao, X.-L. Sun and M.-G. Zhao, *Neurotherapeutics*, 2013, **10**, 340–353; (c) M. Tian, T. Lan, M. Gao, B. Li, G. Zhang and H.-B. Wang, *Aust. J. Chem.*, 2019, **72**, 492–500.
- 9 (a) R. Tamura, S. Susuki, N. Azuma, A. Matsumoto, F. Toda, A. Kamimura and K. Hori, *Angew. Chem., Int. Ed. Engl.*, 1994, **33**, 878–879; (b) M. Minguet, D. B. Amabilino, K. Wurst and J. Veciana, *J. Solid State Chem.*, 2001, **159**, 440–450.
- 10 (a) G. I. Likhtenshtein, J. Yamauchi, S. Nakatsuji, A. I. Smirnov and R. Tamura, *Nitroxides: Applications in Chemistry, Biomedicine, and Materials Science*, Wiley-VCH, Weinheim, 2008, ch. 9, pp. 303–329; (b) H. Wang, P. Gao, L. Jing, X. Sun and R. Jiang, *Acta Chim. Slov.*, 2012, **59**, 413–417; (c) D. A. Morozov, I. A. Kirilyuk, D. A. Komarov, A. Goti, I. Y. Bagryanskaya, N. V. Kuratieva and I. A. Grigor'ev, *J. Org. Chem.*, 2012, **77**, 10688–10698; (d) A. D. Milov, Y. D. Tsvetkov, M. Bortolus, A. L. Maniero, M. Gobbo, C. Toniolo and F. Formaggio, *Biopolymers*, 2014, **102**, 40–48; (e) M. De Zotti, K. Wright, E. d'Aboville, A. Toffoletti, C. Toniolo, G. Longhi, G. Mazzeo, S. Abbate and F. Formaggio, *J. Org. Chem.*, 2017, **82**, 10033–10042.
- 11 G. I. Likhtenshtein, *Nitroxides. Brief History, Fundamentals, and Recent Developments*, Springer, Cham, CH, 2020.
- 12 (a) M. Minguet, D. Luneau, C. Paulsen, E. Lhotel, A. Gorski, J. Waluk, D. B. Amabilino and J. Veciana, *Polyhedron*, 2003, **22**, 2349–2354; (b) C. Hirel, J. Pécaut, S. Choua, P. Turek, D. B. Amabilino, J. Veciana and P. Rey, *Eur. J. Org. Chem.*, 2005, 348–359.
- 13 M. Akita-Tanaka, H. Kumagai, A. Markosyan and K. Inoue, *Bull. Chem. Soc. Jpn.*, 2007, **80**, 204–207.
- 14 (a) H. Kumagai and K. A. Inoue, *Angew. Chem., Int. Ed.*, 1999, **38**, 1601–1603; (b) K. Inoue, H. Kumagai and A. S. Markosyan, *Synth. Met.*, 2001, **121**, 1772–1773.
- 15 Y. Numata, K. Inoue, N. Baranov, M. Kurmoo and K. Kikuchi, *J. Am. Chem. Soc.*, 2007, **129**, 9902–9909.
- 16 X. Liu, Y. Zhang, W. Shi and P. Cheng, *Inorg. Chem.*, 2018, **57**, 13409–13414.
- 17 A. A. Patrascu, M. Briganti, S. Soriano, S. Calancea, R. A. Allão-Cassaró, F. Totti, M. G. F. Vaz and M. Andruh, *Inorg. Chem.*, 2019, **58**, 13090–13101.
- 18 R. Tanimoto, S. Suzuki, M. Kozaki, D. Shiomi, K. Sato, T. Takui and K. Okada, *Bull. Chem. Soc. Jpn.*, 2014, **87**, 314–322.
- 19 (a) T.-N. Le, H. Grewal, V. Changoco, V. Truong and D. J. R. Brook, *Tetrahedron*, 2016, **72**, 6368–6374; (b) A. B. Solea, T. Wohlhauser, P. Abbasi, Y. Mongbanziama, A. Crochet, K. M. Fromm, G. Novitchi, C. Train, M. Pilkington and O. Mamula, *Dalton Trans.*, 2018, **47**, 4785–4789.
- 20 For examples of P-containing C-chiral cyclic nitroxyl radicals see: (a) S. Shimono, H. Takahashi, N. Sakai, R. Tamura, N. Ikuma and J. Yamauchi, *Mol. Cryst. Liq. Cryst.*, 2005, **440**, 37–52; (b) A. Hatano, N. Terado, Y. Kanno, T. Nakamura and G. Kawai, *Synth. Commun.*, 2019, **49**, 136–145.
- 21 Phosphates: (a) S. Iwamoto, W. Kai, T. Isogai, T. Saito, A. Isogai and T. Iwata, *Polym. Degrad. Stab.*, 2010, **95**, 1394–1398; (b) I. Sadowska-Bartosz, I. Stefaniuk, B. Cieniek and G. Bartosz, *Free Radical Res.*, 2017, **52**, 335–338
Phosphazenes: (c) E. Badetti, V. Lloveras, J. L. Muñoz-Gómez, R. M. Sebastián, A. M. Caminade, J. P. Majoral, J. Veciana and J. Vidal-Gancedo, *Macromolecules*, 2014, **47**, 7717–7724
Phosphonates: (d) H. Moons, E. Goovaerts, V. P. Gubskaya, I. A. Nuretdinov, C. Corvaja and L. Franco, *Phys. Chem. Chem. Phys.*, 2011, **13**, 3942–3951
Phosphoramidites: (e) C. H. Wunderlich, R. G. Huber, R. Spitzer, K. R. Liedl, K. Kloiber and C. Kreutz, *ACS Chem. Biol.*, 2013, **8**, 2697–2706.
- 22 (a) S. G. Reis, M. A. del Águila-Sánchez, G. P. Guedes, G. B. Ferreira, M. A. Novak, N. L. Speziali, F. López-Ortiz

- and M. G. F. Vaz, *Dalton Trans.*, 2014, **43**, 14889–14901; (b) S. G. Reis, M. A. del Águila-Sánchez, G. P. Guedes, Y. Navarro, R. A. Allão-Cassaró, G. B. Ferreira, S. Calancea, F. López-Ortiz and M. G. F. Vaz, *Polyhedron*, 2018, **144**, 166–175.
- 23 S. G. Reis, M. Briganti, S. Soriano, G. P. Guedes, S. Calancea, C. Tiseanu, M. A. Novak, M. A. del Águila-Sánchez, F. Totti, F. López-Ortiz, M. Andruh and M. G. F. Vaz, *Inorg. Chim. Acta*, 2016, **55**, 11676–11684.
- 24 For recent reviews see: (a) O. I. Kolodiazny, *Top. Curr. Chem.*, 2015, **360**, 161–236; (b) M. Dutartre, J. Bayardon and S. Jugé, *Chem. Soc. Rev.*, 2016, **45**, 5771–5794; (c) Y.-M. Cui, Y. Lin and L.-W. Xu, *Coord. Chem. Rev.*, 2017, **330**, 37–52; (d) G. Xu, C. H. Senanayake and W. Tang, *Acc. Chem. Res.*, 2019, **52**, 1101–1112; (e) A. Cabre, A. Riera and X. Verdaguier, *Acc. Chem. Res.*, 2020, **53**, 676–689.
- 25 (a) M. Casimiro, L. Rocas, S. García-Granda, M. J. Iglesias and F. López-Ortiz, *Org. Lett.*, 2013, **15**, 2378–2381; (b) M. Casimiro, G. P. Guedes, M. J. Iglesias and F. López-Ortiz, *Tetrahedron: Asymmetry*, 2015, **26**, 53–66.
- 26 M. A. del Águila-Sánchez, Y. Navarro, J. García-López, G. P. Guedes and F. López-Ortiz, *Dalton Trans.*, 2016, **45**, 2008–2022.
- 27 Y. Matsuoka, M. Yamato, T. Yamasaki, F. Mito and K.-I. Yamada, *Free Radical Biol. Med.*, 2012, **53**, 2112–2118.
- 28 (a) J. Kollar, P. Hrdlovic and S. Chmela, *J. Photochem. Photobiol., A*, 2009, **204**, 191–199; (b) T. Yang, B. Zheng, H. Liang, Y. Wan, J. Du and D. Xiao, *Talanta*, 2015, **132**, 191–196.
- 29 (a) A. J. G. Baxter and S. J. Teague, *Tetrahedron*, 1993, **49**, 9089–9094; (b) J. Bariwalab and E. van der Eycken, *Chem. Soc. Rev.*, 2013, **42**, 9283–9303.
- 30 M. S. Driver and J. F. Hartwig, *J. Am. Chem. Soc.*, 1996, **118**, 7217–7218.
- 31 F. Y. Kwong, A. Klapars and S. L. Buchwald, *Org. Lett.*, 2002, **4**, 581–584.
- 32 This loss in yield can be associated to the retention of the compound in the silica support used during the purification procedure. (a) H. Zhang and L. Fu, *Synth. Commun.*, 2014, **44**, 610–619; (b) M. Mogharabi-Manzari, M. Amini, M. Abdollahi, M. Khoobi, G. Bagherzadeh and M. A. Faramarz, *ChemCatChem*, 2018, **10**, 1542–1546.
- 33 A search in the Cambridge structural database for Ph₂P(O) NHR fragments provided 78 entries: min/max P–O distances of 1.451/1.506 Å.
- 34 V. Moodley, C. Mthethwa, M. N. Pillay, B. Omondi and W. E. van Zyl, *Polyhedron*, 2015, **99**, 87–95.
- 35 S. Calancea, S. G. Reis, G. P. Guedes, R. A. Allão-Cassaró, F. Semaan, F. López-Ortiz and M. G. F. Vaz, *Inorg. Chim. Acta*, 2016, **453**, 104–114.
- 36 (a) O. P. Anderson and T. C. Keuchler, *Inorg. Chem.*, 1980, **19**, 1417–1422; (b) K. Griesar, W. Haase, I. Svoboda and H. Fuess, *Inorg. Chim. Acta*, 1999, **287**, 181–185; (c) M. Baskett, P. M. Lahti and F. Palacio, *Polyhedron*, 2003, **22**, 2363–2374; (d) R. A. Allão, A. K. Jordão, J. A. L. C. Resende, A. C. Cunha, V. F. Ferreira, M. A. Novak, C. Sangregorio, L. Sorace and M. G. F. Vaz, *Dalton Trans.*, 2011, **40**, 10843–10850; (e) A. V. Artem'ev, O. V. Vysotskaya, L. A. Oparina, A. S. Bogomyakov, S. S. Khutsishvili, I. V. Sterkhova, V. I. Ovcharenko and B. A. Trofimov, *Polyhedron*, 2016, **119**, 293–299.
- 37 F. Lin, D. Pei, W. He, Z. Huang, Y. Huang and X. Guo, *J. Mater. Chem.*, 2012, **22**, 11801–11807.
- 38 (a) J. J. Borrás-Almenar, E. Coronado, J. Curely, R. Georges and J. J. Gianduzzo, *Inorg. Chem.*, 1994, **33**, 5171–5175; (b) G. De Munno, M. Julve, F. Lloret, J. Faus, M. Verdaguier and A. Caneschi, *Inorg. Chem.*, 1995, **34**, 157–165; (c) G. Viau, M. G. Lombardi, G. De Munno, M. Julve, F. Lloret, J. Faus, A. Caneschi and J. M. Clemente-Juan, *Chem. Commun.*, 1997, 1195–1196; (d) N. Marino, D. Armentano, G. De Munno, J. Cano, F. Lloret and M. Julve, *Inorg. Chem.*, 2012, **51**, 4323–4334.
- 39 O. Kahn, *Molecular Magnetism*, VCH Publishers, New York, 1993.
- 40 (a) Y.-L. Gao, S. Nishihara and K. Inoue, *CrystEngComm*, 2018, **20**, 2961–2967; (b) Y. Navarro, G. P. Guedes, J. Cano, P. Ocón, M. J. Iglesias, F. Lloret and F. López-Ortiz, *Dalton Trans.*, 2020, **49**, 6280–6294.
- 41 Bruker, *APEX2 v2014.5-0*, Bruker AXS Inc., Madison, Wisconsin, USA, 2007.
- 42 Bruker, *SAINT*, Bruker AXS Inc., Madison, Wisconsin, USA, 2007.
- 43 Bruker, *SADABS*, Bruker AXS Inc., Madison, Wisconsin, USA, 2001.
- 44 G. M. Sheldrick, *Acta Crystallogr., Sect. A: Found. Crystallogr.*, 2008, **64**, 112–122.
- 45 G. M. Sheldrick, *Acta Crystallogr., Sect. C: Struct. Chem.*, 2015, **71**, 3–8.
- 46 C. F. Macrae, P. R. Edgington, P. McCabe, E. Pidcock, G. P. Shields, R. Taylor, M. Towler and J. van de Streek, *J. Appl. Crystallogr.*, 2006, **39**, 453–457.
- 47 Y. Ou, Y. Huang, Z. He, G. Yu, Y. Huo, X. Li, Y. Gao and Q. Chen, *Chem. Commun.*, 2020, **56**, 1357–1370.